The stable actin core of mechanosensory stereocilia features continuous turnover of actin cross-linkers

Pallabi Roy and Benjamin J. Perrin*
Department of Biology, Indiana University–Purdue University Indianapolis, Indianapolis, IN 46202

ABSTRACT **Stereocilia are mechanosensitive protrusions on the surfaces of sensory hair cells in the inner ear that detect sound, gravity, and head movement. Their cores are composed of parallel actin filaments that are cross-linked and stabilized by several actin-binding proteins, including fascin-2, plastin-1, espin, and XIRP2. The actin filaments are the most stable known, with actin turnover primarily occurring at the stereocilia tips. While stereocilia actin dynamics has been well studied, little is known about the behavior of the actin cross-linking proteins, which are the most abundant type of protein in stereocilia after actin and are critical for stereocilia morphogenesis and maintenance. Here, we developed a novel transgenic mouse to monitor EGFP-fascin-2 incorporation. In contrast to actin, EGFP-fascin-2 readily enters the stereocilia core. We also compared the effect of EGFP-fascin-2 expression on developing and mature stereocilia. When it was induced during hair cell development, we observed increases in both stereocilia length and width. Interestingly, stereocilia size was not affected when EGFP-fascin-2 was induced in adult stereocilia. Regardless of the time of induction, EGFP-fascin-2 displaced both espin and plastin-1 from stereocilia. Altering the actin cross-linker composition, even as the actin filaments exhibit little to no turnover, provides a mechanism for ongoing remodeling and repair important for stereocilia homeostasis.**

Monitoring Editor
Manuel Théry
CEA, Hopital Saint Louis

Received: Mar 29, 2018
Revised: May 25, 2018
Accepted: May 31, 2018

INTRODUCTION

Stereocilia are actin-based protrusions on the apical surfaces of sensory hair cells in the auditory and vestibular system that detect sound, movement, and gravity. Bundles of auditory stereocilia have three rows of increasing height, giving the appearance of a staircase (Tilney *et al.*, 1980). This architecture is necessary for function, as deflection of the bundle toward the tallest row gates mechanotransduction channels located at the tips of stereocilia in the shorter rows, thereby depolarizing the hair cell in response to sound (Beurg *et al.*, 2009; Schwander *et al.*, 2010; Kazmierczak and Muller, 2012). Because hair cells are not renewed in mammals, proper stereocilia homeostasis, including precise regulation of the length of stereocilia, is critical for maintaining the ability to hear.

Establishment and maintenance of proper stereocilia length depends on regulation of the actin core. The actin filaments within the core are uniformly oriented with their barbed, fast-growing ends toward the stereocilia tip (Flock and Cheung, 1977). These filament ends are relatively dynamic, with polymerization at the tip driving stereocilia elongation during the growth phase (Drummond *et al.*, 2015). Actin continues to incorporate at the tips of mature stereocilia that maintain a constant length, implying that there is ongoing monomer exchange at filament barbed ends (Zhang *et al.*, 2012; Narayanan *et al.*, 2015). Actin along the mammalian stereocilia shaft is exceptionally stable, with little to no detectable actin incorporation (Zhang *et al.*, 2012; Drummond *et al.*, 2015; Narayanan *et al.*, 2015), which contrasts with a previously accepted model where actin was continuously renewed by treadmilling (Schneider *et al.*, 2002; Rzadzinska *et al.*, 2004). While several studies have focused on stereocilia actin dynamics, less is known about the behavior of actin–cross linking proteins, which are abundant in stereocilia.

Several different actin–cross linking proteins are found in stereocilia, including fascin-2 (FSCN2), espin (ESPN), plastin-1 (PLS1), and XIRP2, and contribute significantly to stereocilia development and

This article was published online ahead of print in MBoC in Press (http://www.molbiolcell.org/cgi/doi/10.1091/mbc.E18-03-0196) on June 6, 2018.

*Address correspondence to: Benjamin J. Perrin (bperrin@iupui.edu).

Abbreviations used: ABR, auditory brainstem response; FRAP, fluorescence recovery after photobleaching; IHC, inner hair cell; OHC, outer hair cell; ROI, region of interest; SEM, scanning electron microscopy.

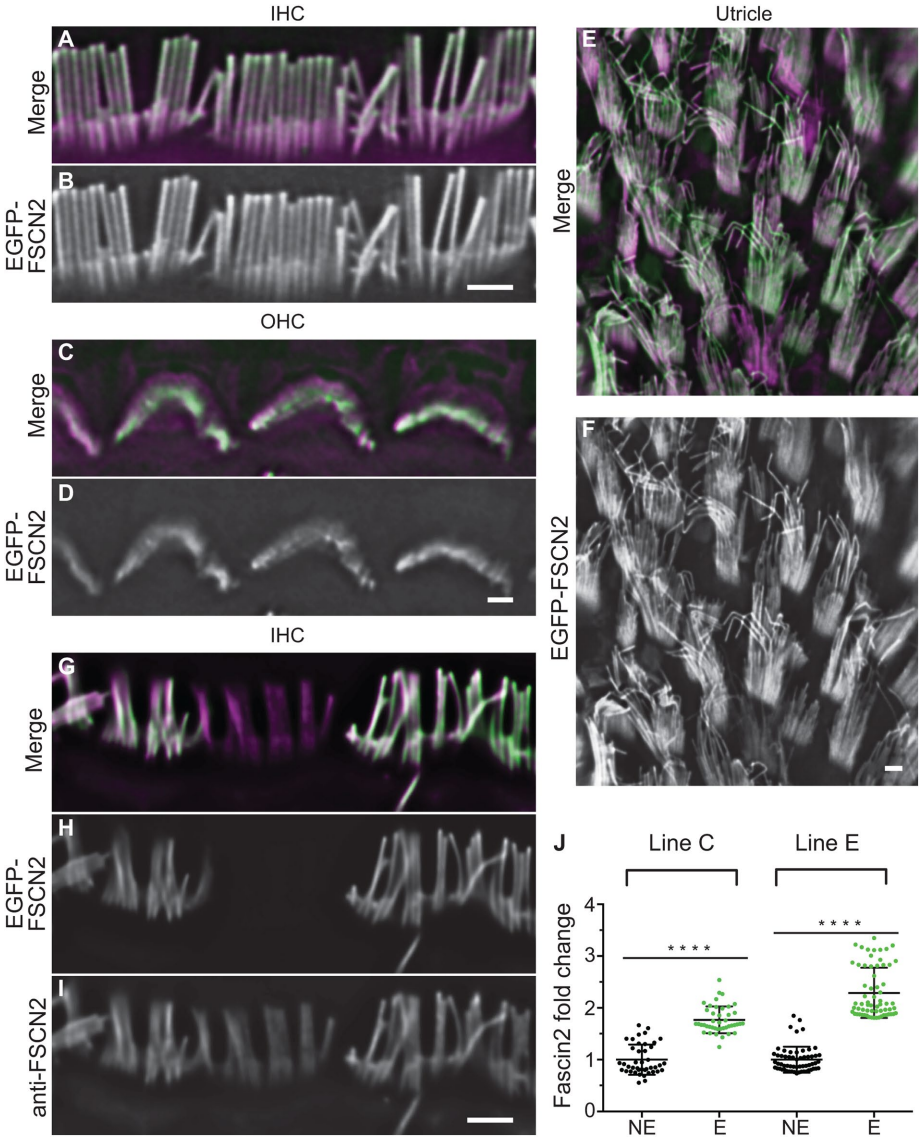

FIGURE 1: EGFP-FSCN2 localized to stereocilia following induction by constitutive Atoh1-Cre. EGFP-FSCN2 localization in IHCs (A, B), OHCs (C, D), and utricular hair cells (E, F) from 4-wk-old mice. F-actin is counterstained with phalloidin. EGFP-FSCN2 is green and phalloidin is magenta in merged images. EGFP-FSCN2 was detected uniformly along the stereocilia length. (G–I) FSCN2 immunostaining in mosaic transgenic line. IHCs from 4-wk-old mice were labeled with anti-FSCN2 antibody (I). EGFP-FSCN2 images (H) show expressing and nonexpressing cells, merged in G. The level of total FSCN2 detected by immunostaining was increased in expressing cells. (J) Plot of the fold change in total FSCN2 levels in lines C and E EGFP-FSCN2 transgenic lines between expressing cells and nonexpressing cells (labeled E and NE). Error bars indicate SD. ****, $p < 0.0001$ (Student's *t* test). Each dot represents one stereocilium ($n \geq 80$ for each condition). Data for each plot were generated from three different mice. Scale bar = 1 μm.

maintenance (Shin *et al.*, 2010; Sekerkova *et al.*, 2011; Perrin *et al.*, 2013; Francis *et al.*, 2015; Scheffer *et al.*, 2015; Taylor *et al.*, 2015). For example, stereocilia in mice expressing mutant FSCN2 protein are initially normal, but subsequently degenerate, and the mice develop progressive hearing loss (Shin *et al.*, 2010). PLS1 is required for stereocilia to grow to their normal width, and also for maintaining stereocilia integrity and function (Taylor *et al.*, 2015). ESPN is also essential for development, as null mutants have abnormally short, thin and unstable stereocilia (Sekerkova *et al.*, 2011). Each of these actin cross-linkers is developmentally regulated in the mouse, with PLS1 and ESPN levels being relatively high as stereocilia are growing, after which their levels decrease. In contrast, the level of FSCN2 increases as stereocilia mature, corresponding to its role in stereocilia maintenance (Shin *et al.*, 2010; Krey *et al.*, 2016).

To characterize FSCN2 incorporation in the mouse, we generated a FLEx-EGFP-FSCN2 transgenic line that allows controlled induction of EGFP-FSCN2 in vivo. We found that, in contrast to actin, EGFP-FSCN2 readily exchanges into the stereocilia core. In addition, EGFP-FSCN2 displaced endogenous PLS1 and ESPN from both mature and developing stereocilia and increased the size of developing, but not mature, stereocilia. Together, these data show that FSCN2 is dynamic and can influence other actin cross-linkers to remodel the highly stable stereocilia actin core.

RESULTS

EGFP-FSCN2 expression early in hair cell development

To monitor EGFP-FSCN2 incorporation in stereocilia in vivo, we developed a new transgenic mouse that allows conditional EGFP-FSCN2 expression following Cre-mediated recombination. Using a FLEx switch (Schnutgen *et al.*, 2003; Schnutgen and Ghyselinck, 2007), recombination excises the tdTomato gene and inverts EGFP-FSCN2 gene so that its expression is now driven by the near-ubiquitous CAGG promoter (Supplemental Figure 1). We characterized three different EGFP-FSCN2 transgenic founder lines by crossing them with the Atoh1-Cre mice, which express Cre recombinase in inner, outer and vestibular hair cells from an early developmental stage (Matei *et al.*, 2005).

Each transgenic founder line (lines C, E, and F) expressed EGFP-FSCN2 to a different extent in hair cells. Line C had a mosaic expression pattern, with detectable EGFP-FSCN2 in ~60% of inner hair cells (IHCs), outer hair cells (OHCs), and utricular hair cells. The other lines showed more penetrant expression, with more than 95% of auditory hair cells expressing in line F (Supplemental Table 1). In all founder lines, EGFP-FSCN2 expression resulted in almost exclusive localization of the protein to stereocilia of OHCs, IHCs, and utricular hair cells and even distribution along the stereocilia length (Figure 1, A–F). EGFP-FSCN2 expression was not detected in mice that lacked the Atoh1-Cre transgene. To measure the extent of EGFP-FSCN2 expression, we performed immunocytochemistry on the sensory epithelium of mosaic lines C and E with dye-conjugated FSCN2 antibody and compared the signal in EGFP-FSCN2 expressing and not expressing IHCs in the same microscopic field (Figure 1, G–I). We found that EGFP-FSCN2 expression increased total FSCN2 levels 1.8-fold in line C and 2.4-fold in line E (Figure 1J).

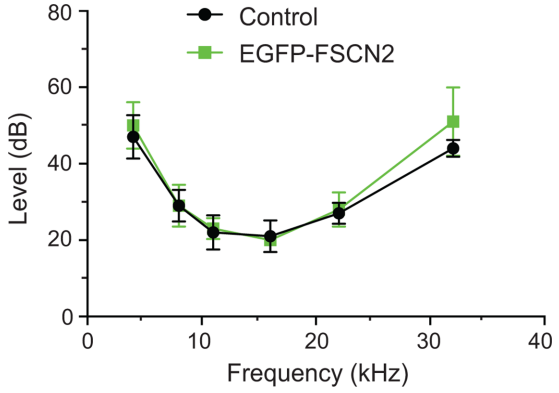

FIGURE 2: EGFP-FSCN2 expression did not perturb auditory function. ABR thresholds from 5-wk-old control mice and transgenic FLEx-EGFP-FSCN2 Atoh1-Cre mice. Error bars indicate SD. For 32 k, $p = 0.9506$, n.s. by Student's t test. Five mice were analyzed for each genotype.

Finally, we tested hearing by measuring auditory brainstem response (ABR) thresholds in line E and F mice, where EGFP-FSCN2 expression was the most penetrant. At 5 wk of age, ABR thresholds of FLEx-EGFP-FSCN2 Atoh1-Cre mice were comparable to those of control mice lacking one or both transgenes, with similar ABR thresholds at all the monitored frequencies (Figure 2). These data indicate that expression of EGFP-FSCN2 does not disrupt stereocilia development or auditory function in young mice.

EGFP-FSCN2 incorporates rapidly into mature stereocilia

To characterize EGFP-FSCN2 incorporation into stereocilia, we irreversibly induced EGFP-FSCN2 expression at P21 by administering tamoxifen to FLEx-EGFP-FSCN2 Cagg-CreER mice, which ubiquitously express the tamoxifen-regulated CreER-recombinase. EGFP-FSCN2 expression was detected uniformly along the entire length of auditory hair cell stereocilia 1 day after induction, which was the earliest time point tested (Figure 3, A and B). EGFP-FSCN2 localized similarly 3 and 7 d postinduction (Figure 3, C–F), and expression was not detected in uninduced control mice (Supplemental Figure 2). For comparison, we used an identical strategy to induce actin-EGFP from a FLEx-actin-EGFP transgene in a separate set of mice. Consistent with previous results, actin-EGFP incorporation in stereocilia was limited to their tips 3 d after induction and could not be detected at earlier time points (Figure 3, G–L; Narayanan *et al.*, 2015). Together, our data demonstrate that in contrast to actin, FSCN2 readily incorporates into stable, established stereocilia cores.

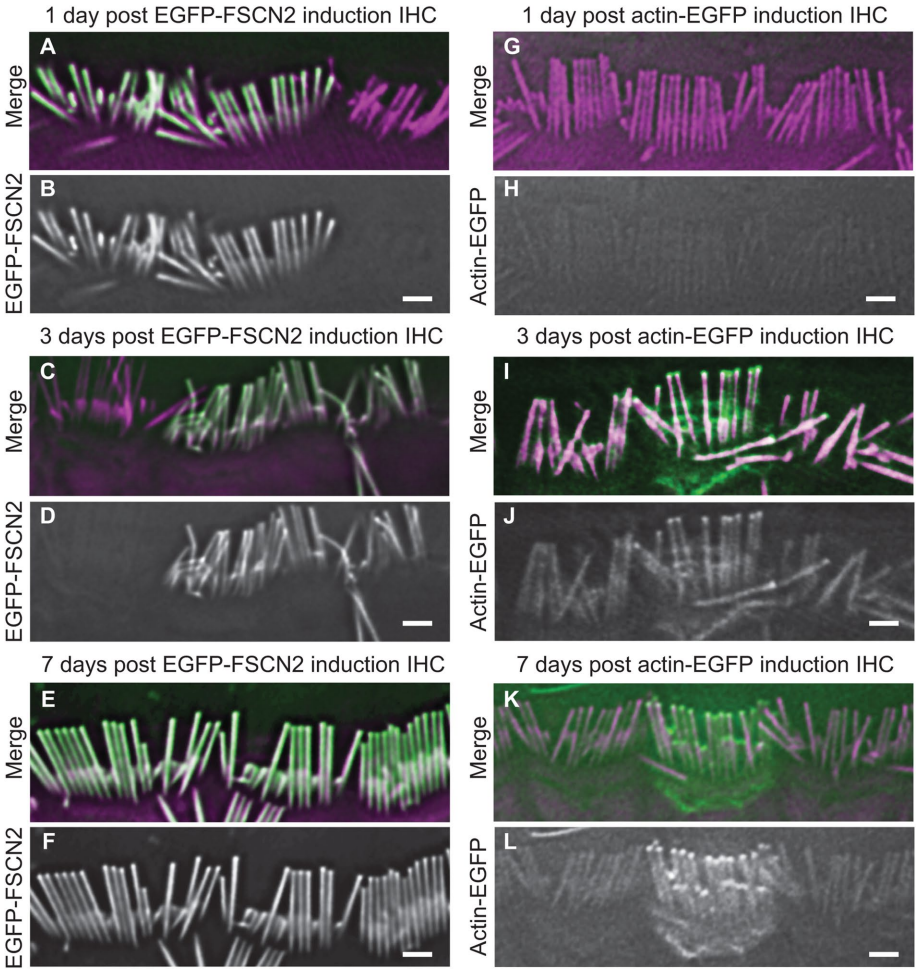

FIGURE 3: Incorporation patterns of EGFP-FSCN2 and actin-EGFP in stereocilia are different. EGFP-FSCN2 (A–F) and actin-EGFP (G–L), merged with phalloidin-stained F-actin 1, 3, or 7 d after tamoxifen was administered to FLEx-EGFP-FSCN2 Cagg-CreER and FLEx-actin-EGFP Cagg-CreER mice. In merged images, EGFP-FSCN2 is green and F-actin is magenta. EGFP-FSCN2 was incorporated along the stereocilia length. In stereocilia, actin-EGFP was restricted to the tips but was also located in the cell body. At least three mice were used for each experiment. Scale bar = 1 μm.

EGFP-FSCN2 incorporation in postnatal explants

To further define the dynamics of EGFP-FSCN2 in stereocilia, we next measured its fluorescence recovery after photobleaching (FRAP) in early postnatal explants. Sensory epithelium was explanted from P7 FLEx-EGFP-FSCN2 Atoh1-Cre mice. Rectangular regions covering about half of inner and outer hair cell bundles were photobleached and EGFP-FSCN2 fluorescence recovery was monitored over time (Figure 4, A and B). The time until half-maximal recovery ($t_{1/2}$) was 7.9 min in OHC stereocilia and 75 min in IHC stereocilia, based on plots of the fraction of fluorescence recovered (Figure 4, C and D). We also quantified fluorescence intensities of the unbleached portion of each bundle. Signal in these regions decreased as fluorescence recovered in the bleached portion (Figure 4, C and D), likely due to movement of EGFP-FSCN2 within the bundle. Thus EGFP-FSCN2 can enter and exit the stereocilia core, and $t_{1/2}$ differs between IHC and OHC stereocilia. For comparison, we also analyzed EGFP-FSCN2 FRAP in utricular stereocilia from the extrastriolar region, which has a mixed population of type I and type II cells. Owing to the different morphology of these bundles, we bleached a smaller rectangular region (Figure 5A).

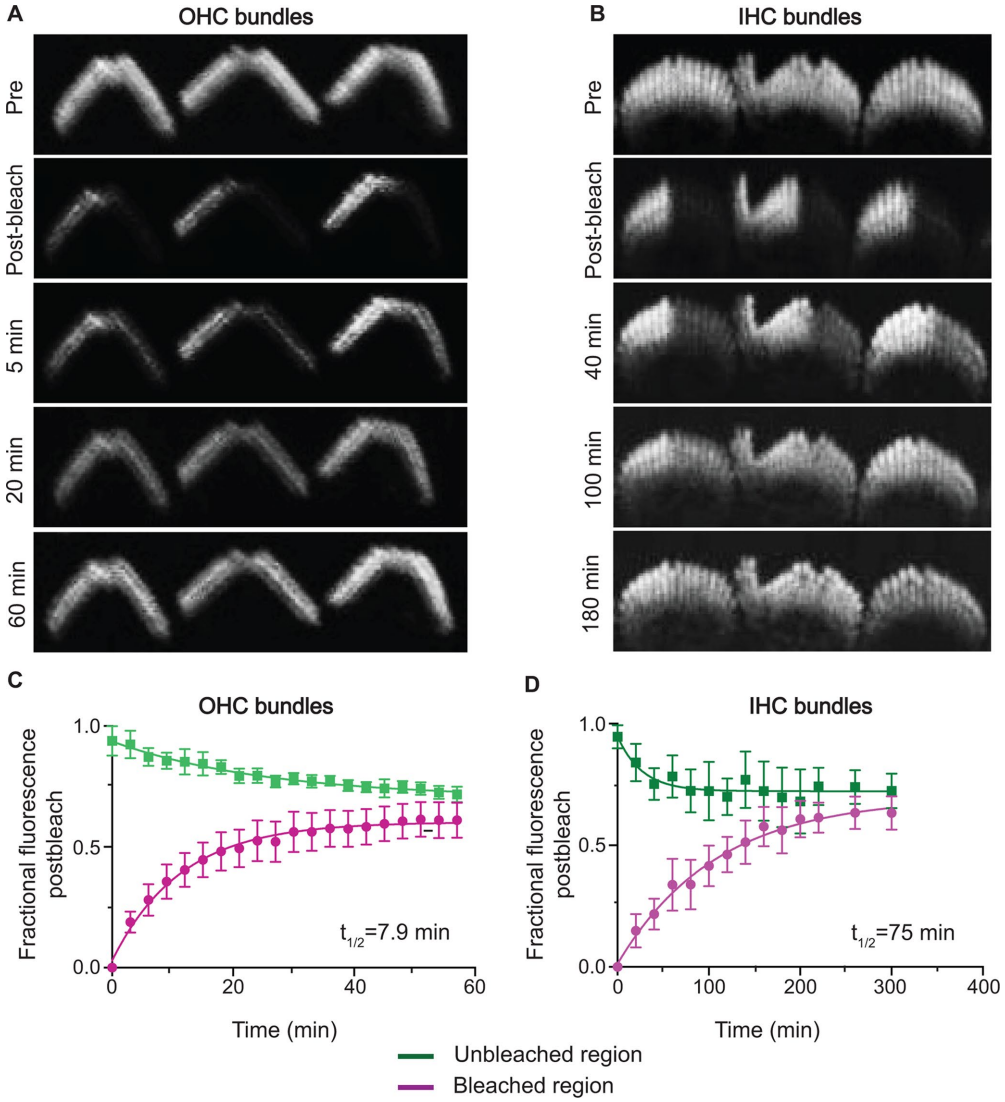

FIGURE 4: EGFP-FSCN2 fluorescence recovery after photobleaching in auditory hair cells. Rectangular regions of stereocilia bundles from P7 FLEx-EGFP-FSCN2 Atoh1-Cre explants were photobleached and fluorescence recovery was monitored over time. (A) OHC bundles. (B) IHC bundles. Plot showing changes in fluorescence intensity from prebleach values within bleached and unbleached sections in OHC (C) and IHC (D) bundles, respectively. The fraction of recovered fluorescence was plotted and fitted with a single exponential curve; $t_{1/2}$ is the time until half-maximal recovery. Error bars indicate SD.

Half-maximal EGFP-FSCN2 recovery took 8.5 min (Figure 5B), which is similar to that of OHC bundles.

PLS1 and ESPN levels in EGFP-FSCN2 transgenic mice

Since FSCN2 cross-links are transient, we reasoned that other stereocilia cross-linkers are likely also dynamic and that EGFP-FSCN2 might compete with them for actin binding within stereocilia. To test this idea, we measured relative PLS1 and ESPN protein levels in EGFP-FSCN2–expressing cells and neighboring nonexpressing cells in the mosaic lines. We first assessed cells in P21-P28 mice, where EGFP-FSCN2 expression was initiated early in development by Atoh1-Cre. Anti-PLS1 antibody and anti-pan-ESPN antibody were used to label stereocilia. With constitutive expression of EGFP-FSCN2, PLS1 levels were decreased ~4-fold and ESPN levels were decreased 2.5-fold in IHC stereocilia expressing EGFP-FSCN2 (Figure 6, A–F, S, and T). EGFP-FSCN2 expression reduced PLS1 (Figure 6, G–I and S) and ESPN (Figure 6, J–L and T) levels ~1.5-fold in OHC stereocilia, while PLS1 and ESPN levels dropped ~3.6-fold (Figure 6, M–O and U) and 1.5-fold, respectively (Figure 6, P–R and V) in utricular stereocilia.

To determine whether FSCN2 can displace PLS1 and ESPN in fully developed IHC stereocilia, we induced FLEx-EGFP-FSCN2 CAGG-CreER at P21. One week postinduction of EGFP-FSCN2 expression, PLS1 levels decreased 1.4-fold while ESPN levels remained nearly stable (Figure 7, A–F, M, and O). Three weeks after EGFP-FSCN2 induction, PLS1 and ESPN levels decreased 3.5- and 1.5-fold, respectively (Figure 7, G–L, N, and P), which is similar to their expression levels when EGFP-FSCN2 was constitutively expressed. These results suggest that EGFP-FSCN2 competes for actin binding with PLS1 and ESPN and are consistent with the idea that actin cross-linkers are remodeled in mature stereocilia.

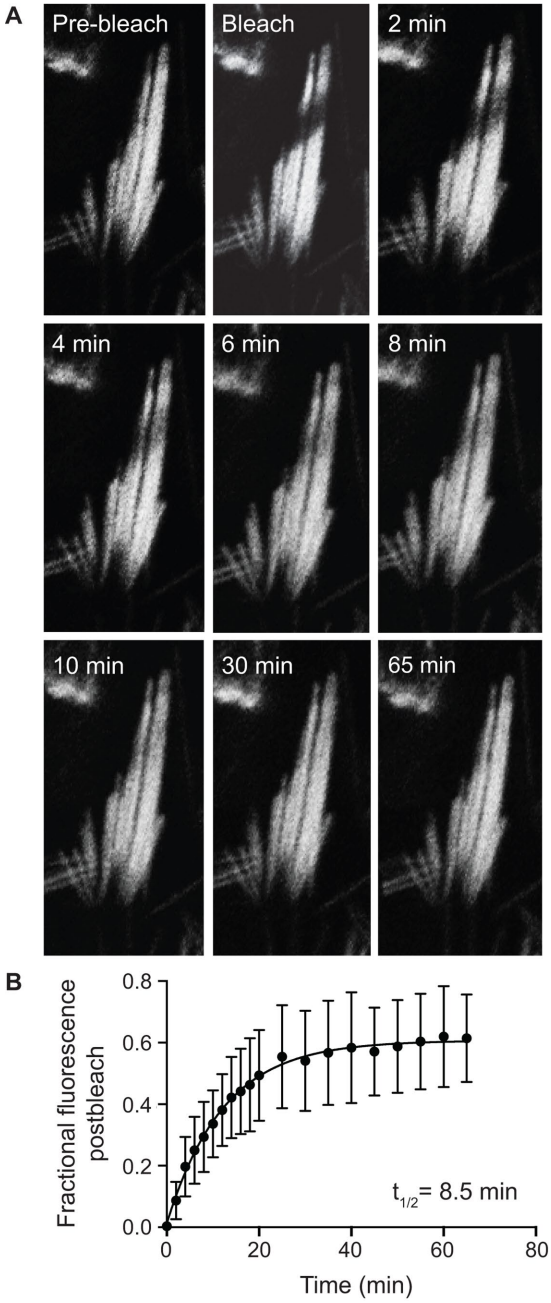

FIGURE 5: Fluorescence recovery of EGFP-FSCN2 after photobleaching in utricular hair cells: (A) Small regions were bleached in P7 FLEx-EGFP-FSCN2 Atoh1-Cre explants and fluorescence recovery was monitored over time until 65 min. (B) Plot showing changes in fluorescence intensity postphotobleaching within the bleached region. The fraction of fluorescence recovered was plotted and fitted with a single exponential curve; $t_{1/2}$ is the time until half-maximal recovery. Error bars indicate SD.

EGFP-FSCN2 expression during hair cell development results in elongation of stereocilia

Next, we wanted to determine whether the altered cross-linker composition resulting from EGFP-FSCN2 expression influences stereocilia architecture. Correlative scanning electron microscopy (SEM) was used to image pairs of expressing and nonexpressing cells identified by fluorescence microscopy in mosaic lines (Supplemental Figure 3). Stereocilia length and width was increased when EGFP-FSCN2 was started early in hair cell development by Atoh1-Cre (Figure 8, A–E). In contrast, initiating EGFP-FSCN2 expression in mature stereocilia at P21 had no apparent effect on stereocilia length or width (Figure 8, F–J). These data show that EGFP-FSCN2 can promote elongation and widening in stereocilia only while they are still growing, but once they are fully developed, the ability of FSCN2 to influence morphology is lost.

DISCUSSION

Mammalian stereocilia are distinguished by the exceptional stability of the actin filaments that compose their cores. Once formed, these filaments appear to be largely static, which contrasts with actin dynamics in structures such as microvilli, filopodia, or lamellipodia, where the actin network turns over rapidly. To gain further insight into the unique behavior of stereocilia cores, we assessed the dynamics of actin cross-linkers in vivo using a new mouse model. We found that actin cross-linkers, which are abundant and required for stereocilia formation and maintenance, are readily exchanged within stereocilia, even though actin filaments are highly stable.

Early studies suggested that actin in stereocilia was continuously renewed by a treadmilling mechanism (Schneider *et al.*, 2002; Rzadzinska *et al.*, 2004). However, recent experiments in the mouse and the bullfrog using several approaches including multi-isotope imaging mass spectrometry (Zhang *et al.*, 2012), conditional actin isoform ablation (Zhang *et al.*, 2012), live imaging of GFP-actin (Drummond *et al.*, 2015), and conditional expression of GFP-actin in vivo (Narayanan *et al.*, 2015) instead demonstrated that actin incorporation is largely restricted to stereocilia tips, where the barbed ends of the filaments terminate. Away from the tip, very little actin is gained or lost along the length of the stereocilia core after it is formed, even over months-long experimental time courses (reviewed in McGrath *et al.*, 2017).

Mammalian stereocilia actin cores are much more stable than those in zebrafish, where actin is reported to turn over on an hourly timescale (Hwang *et al.*, 2015), or the bundled actin filaments that form *Drosophila* bristles, where actin is depolymerized within days of assembly (Otani *et al.*, 2016) Even though actin stability varies markedly between these structures, GFP-fascin isoforms behave similarly. Each isoform is able to incorporate into the existing actin network, suggesting that similar mechanisms drive turnover. However, the half-life of GFP-fascin isoforms in FRAP experiments varies considerably, ranging from seconds in *Drosophila* bristles (Otani *et al.*, 2016) and zebrafish stereocilia (Hwang *et al.*, 2015) to several minutes in mouse stereocilia, where the half-life is 10-fold longer in IHC stereocilia than in OHC stereocilia (Figure 4, C and D). These differences may be due in part to how the actin filaments are packed, which differs according to the complement of actin cross-linkers that are expressed (Krey *et al.*, 2016). For example, IHC stereocilia cores have a central domain of hexagonally packed actin filaments that is lacking in OHC and utricular stereocilia, where filaments instead have a liquid packing arrangement (Krey *et al.*, 2016). Fascin promotes hexagonal packing (Yang *et al.*, 2013) and, considering that fascin-actin binding is cooperative (Winkelman *et al.*, 2016), it may dissociate more slowly in the central region of the IHC core.

Interestingly, expression of EGFP-FSCN2 resulted in decreased levels of ESPN and PLS1 localized to stereocilia, indicating that actin cross-linkers may compete for binding (Figures 6 and 7). Besides competitive binding, crowding, decreased antigen accessibility, or

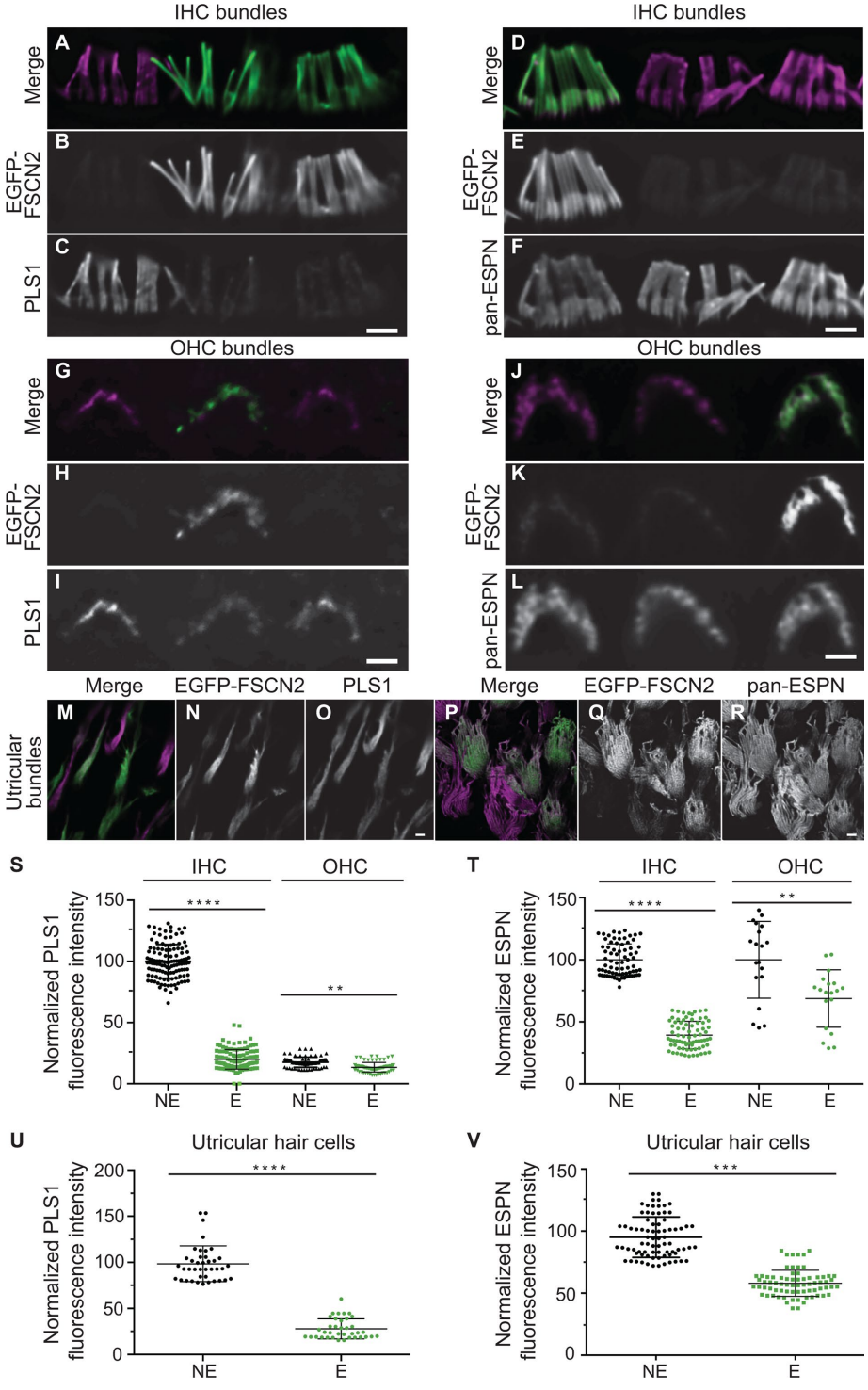

FIGURE 6: Constitutive EGFP-FSCN2 decreases PLS1 and ESPN levels in stereocilia. Anti-PLS1 immunostaining of IHC (A–C), OHC (G–I), and utricular (M–O) stereocilia; anti-pan-ESPN immunostaining of IHC (D–F), OHC (J–L), and utricular (P–R) stereocilia from FLEx-EGFP-FSCN2 Atoh1-Cre at 3 wk of age. Mosaic EGFP-FSCN2 expression allowed comparison of PLS1 or ESPN levels in neighboring cells with or without EGFP-FSCN2 expression. In merged images, EGFP-FSCN2 is green and anti-PLS1 or anti-pan-ESPN staining is magenta. EGFP-FSCN2 expressing cells (marked as E) had PLS1 and ESPN levels lower than the nonexpressing cells (marked as NE) in all the cell types studied here. (S–V) Plots of normalized fluorescence intensity of anti-PLS1 staining in IHC and OHC stereocilia, S, and utricular stereocilia, U, as well as anti-pan-ESPN staining in IHC and OHC stereocilia, T, and utricular stereocilia, V. In S and T, intensity values for nonexpressing and expressing cells (marked NE and E, respectively) were normalized to the average nonexpressing IHC value, and in U and V, to the average nonexpressing utricular value acquired in the same image. Error bars indicate SD; ****, $p < 0.0001$; ***, $p < 0.001$; and **, $p < 0.05$ (one-way analysis of variance). Each dot represents one stereocilium. At least three mice were used for each experiment. Data for each plot were generated from three different mice. Scale bar = 1 µm.

changes in filament conformation that decreased binding site availability or affinity for ESPN or PLS1 may account for their loss from stereocilia. Inducing EGFP-FSCN2 expression early in development or after stereocilia were mature decreased ESPN and PLS1 levels to a similar extent, suggesting that other cross-linkers besides FSCN2 are dynamic and can enter and leave the actin array independent of filament stability. Furthermore, PLS1 levels continued to decrease between 1 and 3 wk following EGFP-FSCN2 induction in mature hair cells, perhaps reflecting slower changes to the packing arrangement of actin filament shifts or normal developmental changes in the endogenous expression levels of cross-linkers (Krey *et al.*, 2016).

Multiple cross-linkers are required for normal stereocilia maintenance, while others are also required for bundle development (reviewed in McGrath *et al.*, 2017). We found that EGFP-FSCN2 increased stereocilia length and width only when it was initiated early in development (Figure 8, A–E) and had no effect on mature stereocilia (Figure 8, F–J). It is likely that FSCN2 slightly increases the stereocilia growth rate, but not the developmental timing of growth. After a developmental shift that prevents further growth, cross-linking is not sufficient to increase stereocilia size. Instead, FSCN2 cross-links, though themselves transient, seem to promote stereocilia stability, as mice expressing mutant FSCN2 form normal stereocilia that subsequently degenerate (Perrin *et al.*, 2013).

Stereocilia maintenance is important, since their integrity is essential for hearing and mammalian hair cells are never replaced. However, potential repair mechanisms are somewhat mysterious, considering that the actin filaments are not detectably replaced, yet are almost certainly damaged by years of mechanical stimulation. How are small breaks in the core fixed? Perhaps transient actin cross-links allow a small amount of actin depolymerization and assembly at sites of damage while still preserving the overall stability of the structure.

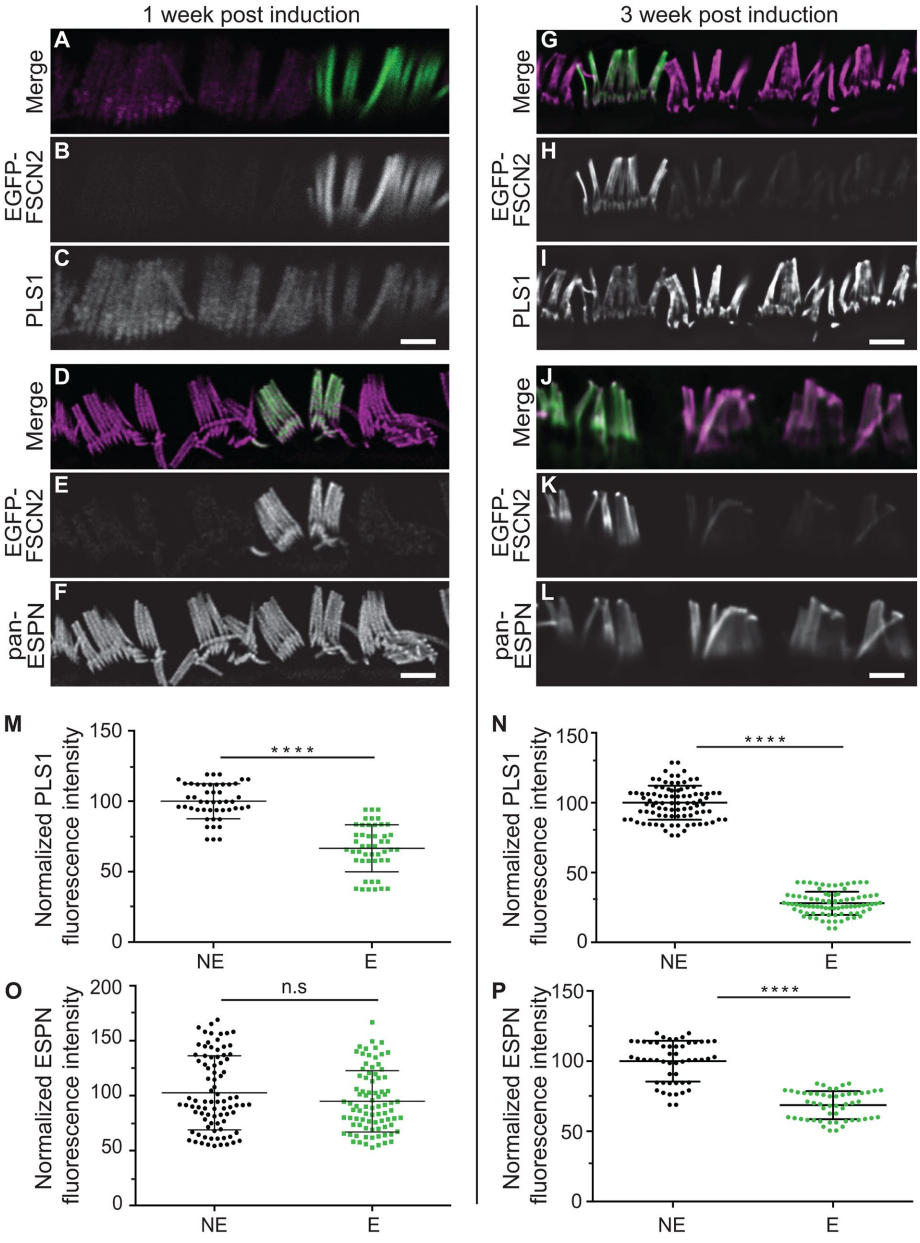

FIGURE 7: Inducing EGFP-FSCN2 expression in IHC stereocilia at P21 reduces PLS1 and ESPN levels. One week (A–F) and 3 wk (G–L) after EGFP-FSCN2 expression was started by Cre mediated recombination. Immunostaining of PLS1 (C, I) and pan-ESPN (F, L) while EGFP-FSCN2 fluorescence marks expressing cells (B, E, H, K). In merged images, PLS1 and pan-ESPN staining is magenta and EGFP-FSCN2 is green. (M–P) Fluorescence intensity of PLS1 and pan-ESPN staining was normalized to the average value of nonexpressing cells in the same image. Nonexpressing and expressing cells are labeled NE and E, respectively, on the *x*-axes. Plots are PLS1 intensities 1 wk (M) and 3 wk (N) postinduction; pan-ESPN intensities 1 wk (O) and 3 wk (P) postinduction. Error bars indicate SD; ****, $p < 0.0001$, and n.s., not significant ($p > 0.05$; Student's *t* test). Each dot represents one stereocilium, and three mice were analyzed for each experiment. Scale bar = 1 µm.

MATERIALS AND METHODS

Mouse lines

The FLEx-EGFP-FSCN2 construct was generated by cloning the mouse EGFP-FSCN2 sequence into a base FLEx vector. The sequence elements are in the following order: chicken β-actin promoter/intron, lox2372, tdTomato, and lox511 in the forward orientation, followed by β-actin-EGFP, lox2372, and lox511 in the reverse orientation before an SV40 polyA signal in the forward orientation. Linear, gel-purified DNA was injected into C57BL/6 pronuclei, which were implanted into pseudopregnant mice by the Mouse Genetics Core at the Scripps Research Institute. Mice carrying the transgene were identified by PCR analysis of genomic DNA from tail snips. Subsequent generations were maintained on the C57Bl/6 background. Atoh1-Cre and Cagg-CreER lines were as previously described (Perrin *et al.*, 2010; Narayanan *et al.*, 2015). Mouse lines were maintained using standard husbandry practices in AALAC-accredited facilities. The Institutional Animal Care and Use Committee of Indiana University–Purdue University School of Science approved all experimental procedures.

Imaging by fluorescence microscopy

Dissected cochleae were fixed in 4% formaldehyde in phosphate-buffered saline (PBS) for 16 h at 4°C before decalcification in 170 mM EDTA in PBS for 16 h at 4°C. Cochlear turns and the utricle were dissected, incubated in 0.2% Triton X-100 for 10 min, and stained with phalloidin conjugated to Alexa-647 (ThermoFisher). For immunostaining with anti-PLS1, pan-ESPN (recognizing espin 1, 2B, 3A, and 4; Zheng *et al.*, 2014), or FSCN2 antibodies, dissected cochleae were fixed in 4% formaldehyde in PBS for 20 min. The apical cochlear turn was immediately dissected, incubated in 0.5% Triton X-100 for 10 min, blocked in 5% goat serum for 1 h, and incubated with primary antibody overnight at 4°C. Antibodies were anti-FSCN2 dye conjugated to Alexa-546 (1:50; Perrin *et al.*, 2013), anti-PLS1 (1:100; Abnova) raised in mouse, or anti-pan-ESPN (50 µg/ml; a kind gift from James Bartles, Northwestern University) raised in rabbit. Unlabeled primary antibodies were detected with secondary antibodies conjugated to Alexa 546 and F-actin was counterstained with phalloidin-647. Samples were mounted in Prolong Gold and imaged either with a Nikon 90i epifluorescence microscope equipped with a Hamamatsu Orca Flash4-LT CMOS camera, a SOLA-SE II LED illuminator, and a 100X NA 1.45 objective or with a 63X NA 1.4 objective on a Leica SP8 confocal microscope operating in resonant mode. Images were subsequently deconvolved using Huygens X11 Essentials deconvolution software.

Scanning electron microscopy

To assess the effect of EGFP-FSCN2 on stereocilia length, pairs of expressing and nonexpressing cells were identified by fluorescence microscopy before tissue was processed for SEM. Pairs of cells were

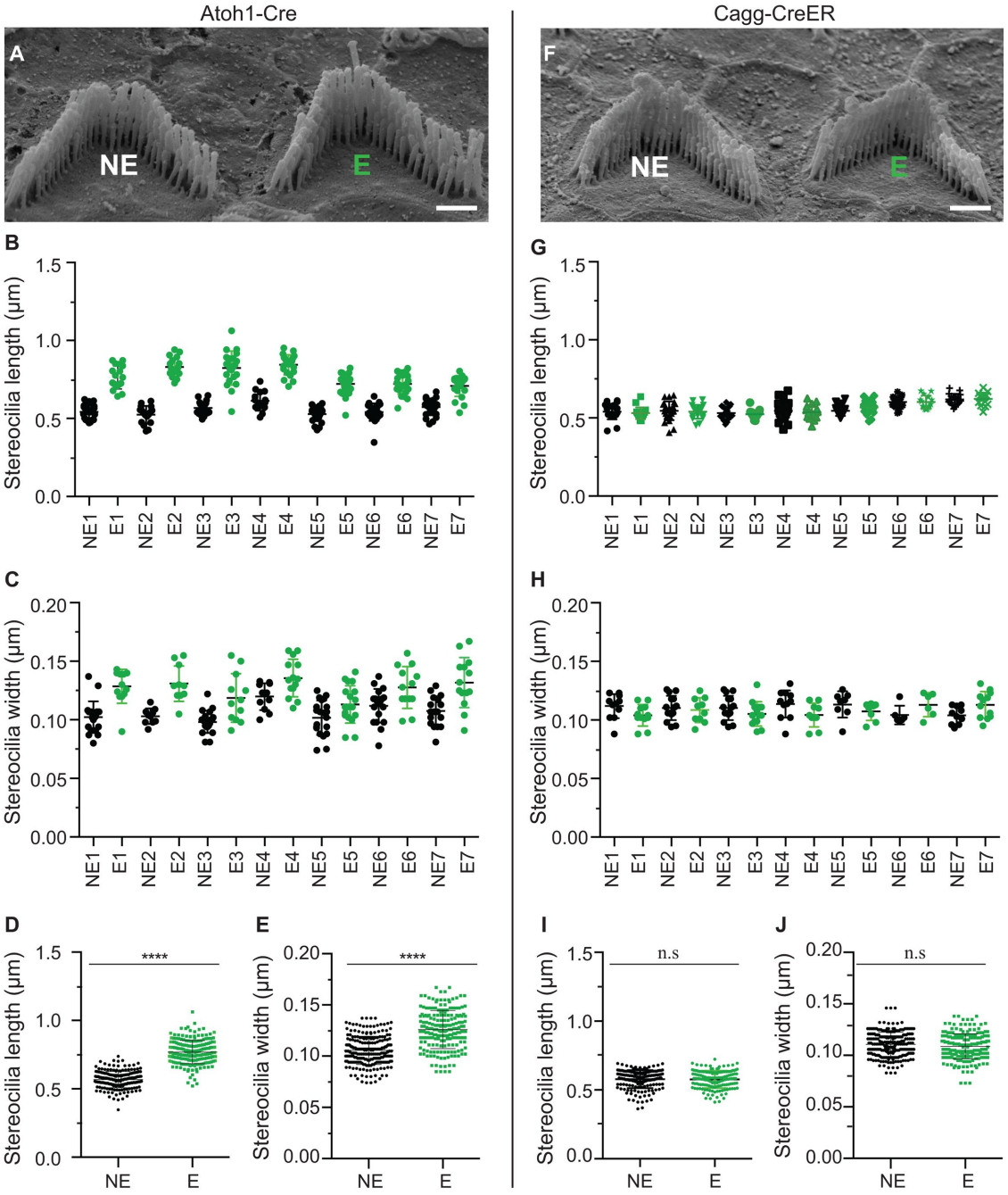

FIGURE 8: EGFP-FSCN2 expression promotes growth of developing but not mature stereocilia. (A–E) OHC stereocilia from 3-wk-old FLEx-EGFP-FSCN2 Atoh1-Cre mice, which express EGFP-FSCN2 from an early developmental stage. (F–J) OHC stereocilia from FLEx-EGFP-FSCN2 Cagg-CreER mice 3 wk after tamoxifen administration to induce EGFP-FSCN2 expression. Pairs of cells where one cell was nonexpressing and the other expressing EGFP-FSCN2 (marked NE and E, respectively) were identified by fluorescence microscopy prior to the processing of the sample for SEM. The identical pairs of cells were located and imaged by SEM (A, F). Lengths and widths of stereocilia in the shortest row of the bundle were measured from cells induced by Atoh1-Cre (B–E) and Cagg-CreER (G–J). Length (B, G) and width (C, H) of pairs of nonexpressing and expressing cells from a single experiment (marked NE and E, respectively). Length (D, I) and width (E, J) collected from three independent experiments. Error bars indicate SD; ****, $p < 0.0001$, and n.s., not significant ($p > 0.05$; Student's t test). Each dot represents one stereocilium, and three mice were analyzed for each experiment. Scale bar = 1 µm

relocated based on comparison of distinctive landmarks in the tissue. Dissected cochlear turns were prepared as for fluorescence microscopy, suspended in a dish of PBS, and imaged using either an upright Nikon 90i epifluorescence microscope or an inverted Leica SP8 laser scanning confocal microscope equipped with a 40× NA 1.1 water immersion objective operating in resonant mode. The turns were then postfixed overnight at 4°C in 2.5% glutaraldehyde, 0.1 M sodium cacodylate, and 2 mM $CaCl_2$. To reduce surface

charging, tissue was incubated overnight at room temperature in 2% each of arginine, glutamine, glycine, and sucrose in water, followed by incubation in 2% tannic acid and guanidine hydrochloride for 2 h at room temperature and then in 1% OsO_4 in water for 1 h at room temperature, with washes in water between each solution. The samples were then transitioned to 100% ethanol, critical point dried from CO_2, and sputter coated with gold before imaging using a JEOL/FE JSM-7800F field emission scanning electron microscope. The stereocilia length and number measurements were analyzed using Fiji software.

Auditory brainstem response

ABR waveforms were collected as previously described (Perrin *et al.*, 2010, 2013) for frequencies of 4, 11, 16, 22, and 32 kHz. A Tucker-Davis Technologies System 3 was used to generate symmetrically shaped tone bursts 1 ms in duration with 300-µs raised cosine ramps that were delivered to a calibrated magnetic speaker starting at suprathreshold levels and decreasing in 5-dB steps to a subthreshold level. Mice were anesthetized with Avertin and scalp potentials were recorded with subdermal electrodes with signals amplified 20,000 times, bandpass filtered between 0.03 and 10 kHz, digitized using a 20,000-kHz sampling rate, and subjected to artifact rejection. The collected waveforms were stacked and the lowest level of stimulation that resulted in a definite waveform was considered as the threshold.

Fluorescence recovery after photobleaching

Middle turns of cochleae were dissected in DMEM:F12 (Thermo Fisher Scientific) from P7 pups constitutively expressing EGFP-FSCN2 transgene and adhered to coverslips coated with Matrigel (Thermo Fisher Scientific). The explants were incubated for 1.5 h at 5% CO_2 and 37°C before the media were exchanged for DMEM (Thermo Fisher Scientific), 7% fetal bovine serum (FBS), and 1 µg/µl of ampicillin. Explants were incubated overnight under the same conditions. The following day, explants were returned to DMEM:F12, inverted on a glass-bottomed dish (Eppendorf) so that the coverslip was supported on spacers, suspending the explant with stereocilia oriented down, and imaged with an inverted laser scanning confocal microscope (Olympus Fluoview1000, 40× NA1.1 water immersion objective). A rectangular region covering approximately half of the hair cell bundle was bleached using a 488-nm laser at 100% power. Fluorescence recovery of EGFP-FSCN2 was monitored by imaging the same bundles at time points for 60 min (OHCs), 5 h (IHCs), or 65 min (utricular hair cells). Fluorescence intensities were determined in regions of interest (ROIs) using ImageJ software as previously described (Narayanan *et al.*, 2015). ROI1 is the bleached region of the bundle, ROI2 is the unbleached region of the bleached bundle, and ROI3 is a region from an unbleached bundle in the same field. The plotted fractional fluorescence recovery values of EGFP-FSCN2 was calculated using the equation $[\{ROI1_x \times (ROI3_{pre}/ROI3_x)\} - \{ROI1_0 \times (ROI3_{pre}/ROI3_0)\}]/(ROI1_{pre} - ROI_0)$, where $ROI1_{pre}$ is before bleaching, ROI_0 is immediately postbleach, and $ROI1_x$ is at time *x*. Similarly, $ROI3_{pre}$ is before bleaching, $ROI3_0$ is immediately postbleach, and $ROI3_x$ is at time *x*. ROI3 serves to correct the intensities of ROI1 and ROI2 for fading that occurred during time-lapse imaging. The time until half-maximal recovery ($t_{1/2}$) was calculated from a fitted curve (one-phase decay function) in GraphPad Prism software. Fractional loss of fluorescence of EGFP-FSCN2 was calculated using the equation $1 - [\{ROI2_{pre} - (ROI2_x \times (ROI3_{pre}/ROI3_x)\}/ROI2_{pre}]$, where $ROI2_{pre}$ is before bleaching and $ROI2_x$ is at time *x*.

ACKNOWLEDGMENTS

We thank Nicolas Berbari (Indiana University–Purdue University Indianapolis) and Melanie Barzik (National Institute on Deafness and Other Communication Disorders) for advice on our manuscript. This work was supported by National Institutes of Health Grant DC015495 to B.J.P.

REFERENCES

Beurg M, Fettiplace R, Nam JH, Ricci AJ (2009). Localization of inner hair cell mechanotransducer channels using high-speed calcium imaging. Nat Neurosci 12, 553–558.

Drummond MC, Barzik M, Bird JE, Zhang DS, Lechene CP, Corey DP, Cunningham LL, Friedman TB (2015). Live-cell imaging of actin dynamics reveals mechanisms of stereocilia length regulation in the inner ear. Nat Commun 6, 6873.

Flock A, Cheung HC (1977). Actin filaments in sensory hairs of inner ear receptor cells. J Cell Biol 75, 339–343.

Francis SP, Krey JF, Krystofiak ES, Cui R, Nanda S, Xu W, Kachar B, Barr-Gillespie PG, Shin JB (2015). A short splice form of Xin-actin binding repeat containing 2 (XIRP2) lacking the Xin repeats is required for maintenance of stereocilia morphology and hearing function. J Neurosci 35, 1999–2014.

Hwang P, Chou SW, Chen Z, McDermott BM Jr (2015). The stereociliary paracrystal is a dynamic cytoskeletal scaffold in vivo. Cell Rep 13, 1287–1294.

Kazmierczak P, Muller U (2012). Sensing sound: molecules that orchestrate mechanotransduction by hair cells. Trends Neurosci 35, 220–229.

Krey JF, Krystofiak ES, Dumont RA, Vijayakumar S, Choi D, Rivero F, Kachar B, Jones SM, Barr-Gillespie PG (2016). Plastin 1 widens stereocilia by transforming actin filament packing from hexagonal to liquid. J Cell Biol 215, 467–482.

Matei V, Pauley S, Kaing S, Rowitch D, Beisel KW, Morris K, Feng F, Jones K, Lee J, Fritzsch B (2005). Smaller inner ear sensory epithelia in Neurog 1 null mice are related to earlier hair cell cycle exit. Dev Dyn 234, 633–650.

McGrath J, Roy P, Perrin BJ (2017). Stereocilia morphogenesis and maintenance through regulation of actin stability. Semin Cell Dev Biol 65, 88–95.

Narayanan P, Chatterton P, Ikeda A, Ikeda S, Corey DP, Ervasti JM, Perrin BJ (2015). Length regulation of mechanosensitive stereocilia depends on very slow actin dynamics and filament-severing proteins. Nat Commun 6, 6855.

Otani T, Ogura Y, Misaki K, Maeda T, Kimpara A, Yonemura S, Hayashi S (2016). IKKepsilon inhibits PKC to promote Fascin-dependent actin bundling. Development 143, 3806–3816.

Perrin BJ, Sonnemann KJ, Ervasti JM (2010). beta-Actin and gamma-actin are each dispensable for auditory hair cell development but required for stereocilia maintenance. PLoS Genet 6, e1001158.

Perrin BJ, Strandjord DM, Narayanan P, Henderson DM, Johnson KR, Ervasti JM (2013). beta-Actin and fascin-2 cooperate to maintain stereocilia length. J Neurosci 33, 8114–8121.

Rzadzinska AK, Schneider ME, Davies C, Riordan GP, Kachar B (2004). An actin molecular treadmill and myosins maintain stereocilia functional architecture and self-renewal. J Cell Biol 164, 887–897.

Scheffer DI, Zhang DS, Shen J, Indzhykulian A, Karavitaki KD, Xu YJ, Wang Q, Lin JJ, Chen ZY, Corey DP (2015). XIRP2, an actin-binding protein essential for inner ear hair-cell stereocilia. Cell Rep 10, 1811–1818.

Schneider ME, Belyantseva IA, Azevedo RB, Kachar B (2002). Rapid renewal of auditory hair bundles. Nature 418, 837–838.

Schnutgen F, Doerflinger N, Calleja C, Wendling O, Chambon P, Ghyselinck NB (2003). A directional strategy for monitoring Cre-mediated recombination at the cellular level in the mouse. Nat Biotechnol 21, 562–565.

Schnutgen F, Ghyselinck NB (2007). Adopting the good reFLEXes when generating conditional alterations in the mouse genome. Transgenic Res 16, 405–413.

Schwander M, Kachar B, Muller U (2010). Review series: the cell biology of hearing. J Cell Biol 190, 9–20.

Sekerkova G, Richter CP, Bartles JR (2011). Roles of the espin actin-bundling proteins in the morphogenesis and stabilization of hair cell stereocilia revealed in CBA/CaJ congenic jerker mice. PLoS Genet 7, e1002032.

Shin JB, Longo-Guess CM, Gagnon LH, Saylor KW, Dumont RA, Spinelli KJ, Pagana JM, Wilmarth PA, David LL, Gillespie PG, Johnson KR (2010). The R109H variant of fascin-2, a developmentally regulated actin cross-linker in hair-cell stereocilia, underlies early-onset hearing loss of DBA/2J mice. J Neurosci 30, 9683–9694.

Taylor R, Bullen A, Johnson SL, Grimm-Gunter EM, Rivero F, Marcotti W, Forge A, Daudet N (2015). Absence of plastin 1 causes abnormal maintenance of hair cell stereocilia and a moderate form of hearing loss in mice. Hum Mol Genet 24, 37–49.

Tilney LG, Derosier DJ, Mulroy MJ (1980). The organization of actin filaments in the stereocilia of cochlear hair cells. J Cell Biol 86, 244–259.

Winkelman JD, Suarez C, Hocky GM, Harker AJ, Morganthaler AN, Christensen JR, Voth GA, Bartles JR, Kovar DR (2016). Fascin- and alpha-actinin-bundled networks contain intrinsic structural features that drive protein sorting. Curr Biol 26, 2697–2706.

Yang S, Huang FK, Huang J, Chen S, Jakoncic J, Leo-Macias A, Diaz-Avalos R, Chen L, Zhang JJ, Huang XY (2013). Molecular mechanism of fascin function in filopodial formation. J Biol Chem 288, 274–284.

Zhang DS, Piazza V, Perrin BJ, Rzadzinska AK, Poczatek JC, Wang M, Prosser HM, Ervasti JM, Corey DP, Lechene CP (2012). Multi-isotope imaging mass spectrometry reveals slow protein turnover in hair-cell stereocilia. Nature 481, 520–524.

Zheng L, Beeler DM, Bartles JR (2014). Characterization and regulation of an additional actin-filament-binding site in large isoforms of the stereocilia actin-bundling protein espin. J Cell Sci 127, 1306–1317.